doi:10.1093/brain/awy206 BRAIN 2018: 141; 2655–2669 | 2655

BRAIN
A JOURNAL OF NEUROLOGY

Functional segregation of basal ganglia pathways in Parkinson's disease

Wolf-Julian Neumann,[1] Henning Schroll,[1] Ana Luisa de Almeida Marcelino,[1] Andreas Horn,[1] Siobhan Ewert,[1] Friederike Irmen,[1,2,3] Patricia Krause,[1] Gerd-Helge Schneider,[4] Fred Hamker[5] and Andrea A. Kühn[1,6,7]

Dopamine exerts modulatory signals on cortex–basal ganglia circuits to enable flexible motor control. Parkinson's disease is characterized by a loss of dopaminergic innervation in the basal ganglia leading to complex motor and non-motor symptoms. Clinical symptom alleviation through dopaminergic medication and deep brain stimulation in the subthalamic nucleus likely depends on a complex interplay between converging basal ganglia pathways. As a unique translational research platform, deep brain stimulation allows instantaneous investigation of functional effects of subthalamic neuromodulation in human patients with Parkinson's disease. The present study aims at disentangling the role of the inhibitory basal ganglia pathways in cognitive and kinematic aspects of automatic and controlled movements in healthy and parkinsonian states by combining behavioural experiments, clinical observations, whole-brain deep brain stimulation fibre connectivity mapping and computational modelling. Twenty patients with Parkinson's disease undergoing subthalamic deep brain stimulation and 20 age-matched healthy controls participated in a visuomotor tracking task requiring normal (automatic) and inverted (controlled) reach movements. Parkinsonian patients on and off deep brain stimulation presented complex patterns of reaction time and kinematic changes, when compared to healthy controls. Stimulation of cortico-subthalamic fibres was correlated with reduced reaction time adaptation to task demand, but not kinematic aspects of motor control or alleviation of Parkinson's disease motor signs. By using clinically, behaviourally and fibre tracking informed computational models, our study reveals that loss of cognitive adaptation can be attributed to modulation of the hyperdirect pathway, while kinematic depends on suppression of indirect pathway activity. Our findings suggest that hyperdirect and indirect pathways, converging in the subthalamic nucleus, are differentially involved in cognitive aspects of cautious motor preparation and kinematic gain control during motor performance. Subthalamic deep brain stimulation modulates but does not restore these functions. Intelligent stimulation algorithms could re-enable flexible motor control in Parkinson's disease when adapted to instantaneous environmental demand. Our results may inspire new innovative pathway-specific approaches to reduce side effects and increase therapeutic efficacy of neuromodulation in patients with Parkinson's disease.

1 Movement Disorder and Neuromodulation Unit, Department of Neurology, Charité Campus Mitte, Charité – Universitätsmedizin Berlin, Berlin, 10117, Germany
2 Department of Biological Psychology and Cognitive Neuroscience, Freie Universität Berlin, Germany
3 Berlin School of Mind and Brain, Humboldt-Universitaet zu Berlin, Germany
4 Department of Neurosurgery, Charité Campus Mitte, Charité – Universitätsmedizin Berlin, Berlin, 10117, Germany
5 Department of Computer Science, Chemnitz University of Technology, 09111 Chemnitz, Germany
6 Neurocure, Centre of Excellence, Charité – Universitätsmedizin Berlin, Berlin, 10117, Germany
7 DZNE, German Center for Degenerative Diseases, Berlin, 10117, Germany

Correspondence to: Dr Wolf-Julian Neumann, MD
Associate Researcher
Movement Disorders and Neuromodulation Unit
Campus Charité Mitte
Department of Neurology

Received March 6, 2018. Revised May 30, 2018. Accepted June 19, 2018. Advance Access publication August 6, 2018

Charité–Universitätsmedizin Berlin
Chariteplatz 1
10117 Berlin
Germany
E-mail: julian.neumann@charite.de

Keywords: deep brain stimulation; basal ganglia; subthalamic nucleus; motor control; Parkinson's disease

Abbreviations: DBS = deep brain stimulation; SMA = supplementary motor area; STN = subthalamic nucleus; UPDRS = Unified Parkinson's Disease Rating Scale

Introduction

The cortex–basal ganglia–thalamic circuit embodies a crucial network for behavioural control (Albin *et al.*, 1989). Alterations in basal ganglia signalling lead to changes in behaviour and have been frequently reported in diverse neurological and neuropsychiatric disorders characterized by perturbed motor control (DeLong, 1990). Parkinson's disease is the most prevalent basal ganglia disorder and causally linked to a loss of dopaminergic neurons in the substantia nigra pars compacta, resulting in a depletion of dopamine in the striatum. Studies in animal models of dopamine depletion have guided the development of a simplified but still useful circuit model of parkinsonism in which the hypodopaminergic state leads to an imbalance in the prokinetic direct and inhibitory indirect striatal–pallidal pathways through a shift in dopamine dependent firing rate modulation of striatal medium spiny neurons (MSNs) (Albin *et al.*, 1989). Loss of dopamine reduces D1 receptor dependent direct pathway MSN activation and increases D2 receptor dependent indirect pathway MSN inhibition resulting in increased GABAergic pallidal output to the thalamus (Wichmann and DeLong, 1996). The subthalamic nucleus (STN) is part of the indirect pathway and drives pallidal GABAergic output through glutamatergic synapses. High frequency deep brain stimulation (DBS) of the STN was probed to reduce increased firing of the indirect pathway, after the observation that lesioning this nucleus in the MPTP non-human primate model of parkinsonism had beneficial effects (Bergman *et al.*, 1990). Subthalamic DBS is now an established treatment for Parkinson's disease patients with motor complications (Deuschl *et al.*, 2006; Weaver *et al.*, 2009; Schuepbach *et al.*, 2013), but the exact mechanisms of DBS-induced changes in motor and non-motor symptoms remain elusive. The identification of a third, 'hyperdirect' cortico–subthalamic pathway (Nambu *et al.*, 2002) implicated the STN in a cognitive inhibition network that delays behavioural responses in favour of outcome optimization (Aron *et al.*, 2016). Subthalamic DBS is hypothesized to suppress the hyperdirect pathway dependent modulation of subthalamic activity (Frank *et al.*, 2007; Herz *et al.*, 2018), but the cognitive effects in patients with Parkinson's disease have so far not been empirically integrated into a holistic account of DBS effects on cognition, movement control and motor disability. Conceptually, the basal ganglia have been proposed to integrate inhibitory control across motor and non-motor domains in favour of adaptive behaviour (Jahanshahi *et al.*, 2015). Inspired by the rise of cell-type specific optogenetic manipulation that has recently actuated a re-evaluation of classic basal ganglia pathway hypotheses in behaving animals (Lee *et al.*, 2017), we designed a study to disentangle the effects of DBS on cognition and motor performance. The aims of the study were (i) to differentiate cognitive demand dependent STN DBS effects on motor preparation and execution; and (ii) to segregate the hyperdirect versus indirect pathway modulation driving these effects. We demonstrate that subthalamic DBS reduces reaction times only in the condition with higher cognitive inhibitory demand, while movement velocity is globally increased independently of task difficulty. Next, we use fibre tracking to elucidate a cortico–subthalamic connectivity pattern between the supplementary motor area (SMA) and the STN that is linked to the DBS effect on cognitive motor control. Finally, we predict and test differential effects of DBS on the hyperdirect and indirect pathways through alterations in a clinically and fibre tracking informed basal ganglia network model.

Materials and methods

Behavioural experiment

We recruited 20 patients with Parkinson's disease undergoing subthalamic DBS under their usual medication from the movement disorders clinic [18 males, age: 63 ± 1.5 years mean $\pm$ standard error of the mean (SEM)]. Patients with prominent tremor in the dominant hand were excluded from the study, to avoid contamination of kinematic traces through tremulous movements. The clinical details are summarized in Table 1. To account for changes both on and off subthalamic stimulation in patients with Parkinson's disease, a group of 20 age-matched healthy participants was recruited (17 males, age 63 ± 1.7). Furthermore, a group of 10 patients with Parkinson's disease (five males, age 59 ± 1.6; for clinical details see Supplementary Table 1) without DBS were tested after withdrawal (OFF) and administration of a fast-acting levodopa agent (ON) and compared to a subgroup of age and Unified Parkinson's Disease Rating Scale (UPDRS) matched DBS patients (Patients 1, 4, 5, 7, 10, 11 and 16–19) to validate the DBS specificity of the task-specific reaction time reduction. To be able to compare the task findings with reduction in motor

Table 1 Subject details of 20 DBS patients and 20 healthy controls

Healthy controls			Parkinson's disease patients with STN DBS									
ID	Sex	Age	ID	Sex	Age	DD	DS	U off	U on	LEDD	DBS parameters	Medication
1	F	79	1	M	61	8	R	26.5	5	0	R3-, 2.1 mA, L3-, 2.1 mA, 60 µs, 130 Hz	None
2	F	69	2	M	63	19	R	51	25	200	R1-, 3.1 mA, L4- 2.7 mA, 90 µs, 70 Hz	Levodopa
3	M	60	3	F	70	14	L	37.5	11	1315	R2-, 2.4 V, L2-,3- 2.3 V, 90 µs, 70 Hz	Levodopa, pramipexole, amantadine
4	M	53	4	F	65	8	R	36.5	16	700	R1-, 3.8 mA, L1- 3 mA, 60 µs, 130 Hz	Levodopa, rasagiline
5	F	60	5	M	59	14	R	24.5	9.5	800	R2-, 2.6 V, L3-, 2.8 V, 60 µs, 130 Hz	Levodopa, piribedil
6	M	68	6	M	55	19	L	24	10	1600	R5-,6-, 3.1 mA, R4-,5-, 2.1 mA, 60 µs, 130 Hz	Levodopa, rasagiline
7	M	55	7	M	55	7	L	27.5	12.5	632	R4-, 0.8 mA, L4-,1.8 mA, 60 µs, 130 Hz	Levodopa, pramipexole, bupropione
8	M	59	8	M	57	10	R	55	18.5	800	R2-,3-, 2.1 V, L2-,3-,2.2 V, 60 µs, 125 Hz	Levodopa
9	M	52	9	M	74	10	R	17	8	850	R3-, 4.4 mA, L3-, 4.4 mA, 60 µs, 180 Hz	Levodopa
10	M	72	10	M	50	6	L	43	11	0	R3-, 2 mA, L3-, 2 mA, 60 µs, 130 Hz	None
11	M	73	11	M	64	13	L	18	8	500	R2-,3-, 3.8 V, L3-, 4.9 V, 60 µs, 130 Hz	Levodopa
12	M	66	12	M	67	21	L	35	23	157	R1-, 2.4 V, L0-,1-, 2.3 V, 60 µs, 110 Hz	Pramipexole
13	M	58	13	M	73	15	L	27	11	550	R2-, 2.5 mA, L2-, 2.1 mA, 60 µs, 130 Hz	Levodopa, piribedil
14	M	55	14	M	60	12	R	22	10	440	R2-, 1.6 mA, L3-, 1.9 mA, 60 µs, 130 Hz	Levodopa, ropinirole
15	M	63	15	M	62	23	L	31	10	1933	R1-,3-, 4.1 V, L1-,3-, 3. V, 60 µs, 120 Hz	Levodopa, ropinirole, amantadine, tolcapone
16	M	74	16	M	64	15	L	18	5	200	R1-, 4.3 V, L2-, 4.2 V, 60 µs, 150	Ropinirole
17	M	51	17	M	66	9	R	13	7	740	R2-, 1.1 V, L3-, 1.3 V, 60 µs, 100 Hz	Levodopa, ropinirole, rasagiline
18	M	59	18	M	60	12	R	27	12	375	R2- 4.8 V, L3-, 4.6 V, 60 µs, 100 Hz	Levodopa
19	M	69	19	M	71	29	L	14	8	460	R2-,3-, 1.9 V, L2- 1.7 V, 60 µs, 130 Hz	Levodopa, pramipexole, amantadine
20	M	61	20	M	50	11	R	31	3.5	0	R3-, 3.8 mA, L3-, 3.2 mA, 60 µs, 130 Hz	None
-	**3F**	**63.2**	**-**	**2F**	**62.6**	**14**	**10R**	**28.9**	**11.2**	**612.6**	**-**	**-**
-	**-**	**1.7**	**-**	**-**	**1.5**	**1**	**-**	**2.5**	**1.2**	**113.6**	**-**	**-**

Age and disease duration (DD) depicted in years at the time of the experiment. UPDRS-III scores (U off / U on) were collected at the time of the experiment. Levodopa equivalent doses (LEDD) are in milligrams. Mean ± SEM given in the two bottom rows (bold text) where appropriate.
DS = dominant side (L = left, R = right); U off = UPDRS-III off stimulation, U on = UPDRS-III on stimulation.

deficits, all patients were examined for parkinsonian symptoms using the motor part of the UPDRS-III on and off DBS and ON and OFF levodopa in the group of non-DBS patients with Parkinson's disease. The study was approved by the local ethics committee with the standards set by the Declaration of Helsinki. For all participants, written informed consent was obtained before inclusion in the study. All participants engaged in a visuomotor task (Fig. 1A), where they had to steer a cursor using a pen on a digitizing tablet (Intuos Pro, Wacom) to round target areas appearing in one of eight pseudorandomized circularly arranged positions on a 15" computer screen 40 cm in front of them. The task was programmed in MATLAB (The Mathworks, Natick, MA, USA) using the cogent toolbox. Trials started when the cursor position was moved to a central fixation cross. After 3 s without movement a warning cue appeared for 500 ms as a yellow circle surrounding the fixation cross and 500 ms later the target appeared. The subjects could respond immediately after the target appeared. The task included two pen-to-cursor mapping conditions. In the automatic condition (green target), the pen-to-cursor mapping was congruent, while in the controlled condition (red target), the pen-to-cursor mapping was inverted. All participants completed 60 trials of each condition split into blocks of 30 trials (ordered

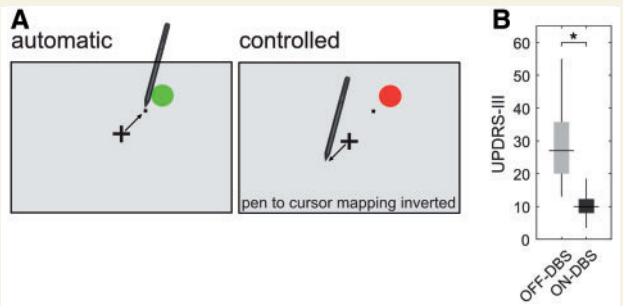

Figure 1 Behavioural task and clinical DBS effect.
Participants engaged in a visuomotor tracking task (**A**) in which a target appeared on one of eight circular positions surrounding the fixation cross to which they had to steer a cursor (little black dot) using a pen on a digitizing tablet in front of the screen. In the automatic condition green targets appeared indicating congruent pen-to-cursor mapping, whereas in the controlled condition pen-to-cursor mapping was inverted. Patients with Parkinson's disease were tested twice, off and on subthalamic DBS, which had a significant effect on clinical motor symptom severity measured with UPDRS-III scores (**B**; box and whisker depict mean, error bars indicate SEM).

block: 4 × 30 trials). The condition was announced before each block, so that the patients could prepare for the pen-to-cursor mapping. The condition of the first block (automatic versus controlled) was randomized across patients and healthy controls. All patients completed the 180 trials twice, once with subthalamic stimulation turned on for at least 30 min and once after subthalamic stimulation was switched off for at least 30 min before task performance. Again, the starting stimulation condition was pseudo-randomized across patients (10 started on stimulation, 10 started off stimulation). Cursor movement traces were saved for offline analysis by converting the concurrent cursor positions in the *x*- and *y*-axes to analogue signals using a National Instruments digital analogue converter (NI-USB 6212; National Instruments) that were recorded on a separate computer using Spike2 software with a 1401 Power Mk2 (CED) A-D converter with a sampling rate of 1000 Hz for offline analysis. All movement traces were analysed using custom MATLAB code. Reaction times were defined as the time between target appearance and the first increase in movement acceleration in either of the two axes. Movement times were defined as the time between movement onset and the cursor reaching the target in each trial. Movement velocity was calculated as the peak of the first derivative of the movement traces. Movement trajectory error was calculated as the average difference between the optimal movement trajectory (straight line) connecting the fixation cross and the target entrance of the cursor interpolated for the length of the movement. Deviation from a straight trajectory leads to increased distance that needs to be covered and is therefore considered less optimal. In a separate block in the same participants, each subject completed 60 trials with conditions pseudo-randomly appearing without prior knowledge of the upcoming trial (random block: 1 × 60 trials). This was designed to validate the generalizability of potential DBS induced reaction time effects to the automatic condition, if the patients are not informed of the pen-to-cursor mapping in advance.

DBS electrode localization and fibre tracking

All patients exhibited satisfactory symptom alleviation through subthalamic DBS with an average improvement in UPDRS-III scores of 60 ± 2.8% on top of medication as assessed during the experiment (Fig. 1B). The DBS electrodes were localized (Fig. 3A) using Lead-DBS (Horn and Kühn, 2015; www.lead-dbs.org) in 19 of 20 patients (Patient 11 was excluded from the fibre tracking analysis because preoperative images were not available for this study, as the patient was operated in another surgical centre). In brief, postoperative images were co-registered to preoperative MRI using SPM12 (http://www.fil.ion.ucl.ac.uk/spm/software/spm12). After visual inspection, co-registrations were manually refined if necessary. Pre- and post-operative acquisitions were spatially normalized into MNI ICBM152 NLIN 2009b stereotactic space using a diffeomorphic registration algorithm using geodesic shooting and Gauss-Neuwton optimization (SHOOT) as implemented in SPM12 (Ashburner and Friston, 2011). SHOOT registration was performed by directly registering tissue segmentations of preoperative acquisitions (obtained using the unified Segmentation approach; (Ashburner and Friston, 2005) to a SHOOT template created from tissue priors defined by the MNI atlas (http://nist.mni.mcgill.ca/?p=904) supplied within Lead-DBS software (Horn and Kühn, 2015; www.lead-dbs.org). Electrodes were localized in the aforementioned MNI space using the semi-automatic implementation in Lead-DBS. Active DBS contacts in the stimulation on condition were then identified and a spherical region of interest with a radius of 1 mm roughly reflecting the cylindrical DBS contacts (1.27 diameter, 1.5 mm length) was created as a seed region projected to an openly available group connectome (www.lead-dbs.org) previously used in Horn *et al.* (2017*b*, *c*), which was derived from diffusion-weighted magnetic resonance images of 90 patients of the Parkinson's progression markers initiative (PPMI) database (Marek, 2011). All scanning parameters are published on the website (www.ppmi-info.org). Whole brain tractography fibre sets were calculated using a generalized q-sampling imaging algorithm as implemented in DSI studio (http://dsi-studio.labsolver.org) within a white-matter mask after segmentation with SPM12. All fibre tracts were transformed into MNI space as previously described (Horn *et al.*, 2014, 2017*c*; Ewert *et al.*, 2018). The current study used connectome data from large cohorts of patients with Parkinson's disease rather than connectivity data from individual patients. This is a major practical advantage, as MRI-based connectivity data are not routinely acquired in DBS patients, making the current results applicable to a greater number of patients with Parkinson's disease, who most often will not have their own connectivity data, and may facilitate generalizability of our approach to other DBS indications (Fox *et al.*, 2014). Beyond this practical advantage, there is also a theoretical advantage in using normative connectome data, which has significantly better signal to noise than data from single patients. Connectome datasets are acquired on special MRI hardware, often with cohort sizes in the thousands, leading to connectivity estimates that are much more robust than those from individual patients. A sensorimotor cortex mask including the SMA and the preSMA was created based on the Automated Anatomical Labeling Atlas (Tzourio-Mazoyer *et al.*, 2002). The hyperdirect pathway was defined by identifying fibres that originate in the sensorimotor cortex and traverse the STN. Fibre tracking gives a relative (and indirect) estimate of potential white matter tracts connecting predefined regions of interest and should not be misunderstood as anatomical truth. Nevertheless, for the sake of simplicity, all fibres identified to connect the STN directly to sensorimotor regions are further denominated as hyperdirect pathway fibres. The amount of fibres affected by stimulation was quantified by identifying hyperdirect pathway fibres traversing the spherical active contact regions of interest for each patient. To investigate the relative change in reaction time adaptation to task condition, the number of hyperdirect pathway fibres was correlated with the subthalamic stimulation related percentage decrease in reaction time adaptation to increased task demand in the controlled condition ($\Delta RToff^{controlled\text{-}automatic} - \Delta RTon^{controlled\text{-}automatic}$) / $\Delta RToff^{controlled\text{-}automatic}$. This measure isolates the specific delay that is induced by the inversion of pen-to-cursor mapping and is robust for the potential effects of improvement in bradykinesia, which could confound a direct comparison of reaction times in the controlled condition off and on DBS. Patients who are able to move faster would have quicker reaction times without a necessary effect of cognitive demand. The relative change was chosen, because patients that were more affected likely are slower to respond, yielding greater absolute reaction time differences. These confounds were nullified by isolating the condition-specific difference in reaction times and quantifying the relative DBS induced change. We refer to this

measure as the relative stimulation induced decrease in reaction time adaptation.

To validate the reported correlation, we further created a voxel-wise structural connectivity correlation map from volumetric fibre density images as previously described in Horn *et al.* (2017*c*). Finally, to identify the most relevant fibres driving the correlation effect, we correlated each fibre density voxel within the sensorimotor cortex mask with the stimulation induced decrease in reaction time adaptation ($\%\Delta RT^{controlled\text{-}automatic}$). Significant ($P < 0.05$) clusters of correlation coefficients in the 3D map were then tested against surrogate clusters derived from random permutation.

Design of the computational basal ganglia model

The architecture of our computational model is shown in Fig. 5A. The model comprises direct, indirect and hyperdirect basal ganglia pathways, connecting SMA to motor cortices via the thalamus. Direct pathway activation facilitates execution of specific motor responses (Go function), while indirect pathway activation inhibits response execution (NoGo function). Hyperdirect pathway activity globally inhibits responding to prevent execution of prepotent responses in the case of response conflict. Next to these basal ganglia pathways, the model contains a cortico-thalamic route that bypasses the basal ganglia to allow for fast execution of highly automatized responses (i.e. in our task, to move towards, but not away from a suddenly appearing stimulus).

The model allows simulating presumed basal ganglia activity *in silico* during patients' execution of the sensorimotor task outlined above. Input stimuli are fed into to the model's supplementary motor cortex. For matters of simplification, we assume the input independent of the particular angle of position in the circular arrangement leading us to only two input locations. The model processes this information and may finally prompt its motor cortex to execute a response (i.e. to move towards or away from the green/ red circle).

Each of the model's structures (i.e. striatum, STN, external and internal globus pallidus, thalamus and motor cortex) comprise two separate units (i.e. artificial neural ensembles) to code for the two possible movement directions (i.e. towards or away from the circle)—except for the supplementary motor cortex, which comprises four individual units to code for four different input stimuli (i.e. red versus green circles, which can each be presented at two different locations).

Spread of activity through the model is visualized in Supplementary Video 1. In brief, presentation of green circles activates both direct and indirect pathways, both of which are directed onto the response towards the circle's locations (hard-coding; no plasticity involved). The balance of direct and indirect pathway activation determines how fast the model's movement towards the circle is executed. Under normal, non-parkinsonian conditions, direct-pathway activation strongly outweighs indirect-pathway inhibition. As there is no response conflict in trials with green circles, moreover, the hyperdirect pathway is only slightly activated. The cortico-thalamic pathway, finally, bypassing the basal ganglia, provides additional facilitation of the movement towards the circle's location (i.e. of the automatized response).

Presentation of red circles similarly activates direct and indirect pathways. However, these are now targeted onto units that encode movement away from the circle. Again, the pathways' balance determines how fast the corresponding movement is executed. Importantly, the cortico–thalamic pathway (encoding automatized movements) now facilitates the competing response to move towards the stimulus (which is incorrect, here), causing response conflict. To prevent prepotent incorrect responses, hyperdirect pathway activation globally inhibits responding.

Each of the model's units is associated with a differential equation (integrated via the Euler method) that determines the unit's membrane potential. In brief, membrane potentials are determined by summing up baseline values, inputs and a random noise term. Membrane potentials are converted into firing rates via a sigmoid function. Detailed descriptions and equations of all model structures are summarized in the Supplementary material.

For fitting purposes, a separate network of our model was run for each human participant that took part in the experiment. Each parkinsonian (i.e. non-healthy) network was informed by the relevant patient's UPDRS score off stimulation as an estimation of how strongly direct and indirect pathways were affected by Parkinson's disease. Parkinson's disease was implemented in the model by additively increasing the strength of the indirect and decreasing the strength of the direct pathway, thereby shifting the balance between speeding up and slowing down movements towards the latter, as also motivated by previous model simulation studies (Schroll *et al.*, 2014; Schroll and Hamker, 2016). The impact of DBS on the STN was determined via two separate factors: first, the patient's empirically determined fibre count value (assumed to be a good estimator of DBS effects on the hyperdirect pathway) and secondly the difference between UPDRS values on and off stimulation (as an estimator of DBS effects on the indirect pathway).

Resulting reaction and movement times of our networks (arbitrary units) were fitted to participants' empirical results. Fitting was achieved by searching for linear transformation parameters (i.e. slope and intercept) that optimally transformed the networks' times into patients' empirical data. To prevent overfitting, only a single slope and intercept value were fitted across trial types for each network.

The model's resulting reaction and movement times were analysed via the same statistical analyses as patients' experimental data.

Statistical analysis

All data are presented as mean ± SEM. All statistical analyses were carried out in MATLAB. To avoid the violation of necessary assumptions, we conducted permutation statistics, whenever possible. These are free from any assumptions about the distributions of group values and are robust against small sample size. Multiple comparisons were corrected by controlling for the false discovery rate (Benjamini *et al.*, 2006) in the behavioural analyses for each measure tested or correlated. As many of the behavioural measures are right skewed, we report non-parametric rank-based Spearman's correlations, whenever possible. If data were normally distributed, we additionally report Pearson's linear correlations. To test for the predictive value of the computational modelling results we conducted linear regression analyses. Therefore, data were transformed to a normal distribution with zero mean and

standard deviation of one, following the approach of van Albada and Robinson (2007). Stepwise model selection was conducted by minimizing the *P*-value in each step. For visualization and reporting of the predictive power of regression analyses, the dependent variable is presented unnormalized, but no results are presented that are not reproducible after data normalization, which generally improved statistical measures. To validate the predictive power of the computational model, we conducted leave one out cross-validation. Therefore, each single value from the observed data were predicted by the linear regression model obtained from the remaining 19 values. This procedure results in pairs of observed and predicted values which can thereafter be tested by classical correlations and permutation tests.

Data availability

The used imaging data in the preparation of this article were obtained from the Parkinson's Progression Markers Initiative (PPMI) database (www.ppmi-info.org/data). The resulting connectome can be reproduced by obtaining the necessary processing code with Lead-DBS (www.lead-dbs.org). Individual patient data will not be distributed openly to conform with data privacy statements signed by all patients. Specific aspects of the dataset can be made available to individuals for academic purposes after assessment through the local data privacy board. The computational models will be made freely available upon request.

Results

Subthalamic stimulation elicits different task-specific effects on cognitive and motor aspects of movement execution

Subthalamic DBS led to a significant improvement of motor symptom severity as measured by the UPDRS-III (Fig. 1B; off: 28.9 ± 2.5, on: 11.2 ± 1.2 points, mean ± SEM reported throughout manuscript; $P < 0.0001$). Patients off stimulation required more time to reach the target after movement onset (from now on referred to as movement time), when compared to healthy controls (Fig. 2A; $P < 0.0001$). This effect was higher in the controlled movement condition with inverted pen-to-cursor mapping ($\Delta MT^{controlled\text{-}automatic}$ $P = 0.002$). DBS decreased movement times ($P < 0.0001$ in both conditions), but movement time was significantly more reduced in the controlled condition ($\Delta MT^{controlled\text{-}automatic}$ $P < 0.0001$). Healthy participants in contrast to patients with Parkinson's disease showed a reduction of movement velocity in the controlled condition (Fig. 2B; $P < 0.0001$). STN stimulation increased movement velocity, but did not improve movement velocity adaptation, leading to less velocity decrease in the controlled condition, when compared to healthy controls ($\Delta V^{controlled\text{-}automatic}$ both off and on stimulation $P < 0.001$, unpaired permutation tests). In line with this, larger trajectory errors (Fig. 2C; defined as the average deviation of the movement trajectory from a straight line connecting the start position with the target) in the on stimulation condition were observed. Importantly, trajectory error was calculated independent of movement time, so that patients with Parkinson's disease who were moving slower could still achieve minimal trajectory errors. Patients with Parkinson's disease off stimulation committed relatively higher movement trajectory errors in the controlled movement condition, when compared to the automatic condition ($\Delta ERR^{controlled\text{-}automatic}$ $P = 0.02$). Subthalamic stimulation increased trajectory errors in both conditions ($P < 0.001$), but again changes were significantly more marked in the controlled condition ($\Delta ERR^{controlled\text{-}automatic}$ $P < 0.005$). Relative movement time changes [$\%MT^{(off\text{-}on)/off}$] correlated significantly with patients' symptom alleviation [$\%UPDRS\text{-}III^{(off\text{-}on)/off}$] across conditions (Spearman's rho = 0.51, $P = 0.01$; Pearson's R = 0.41, $P = 0.03$; both rank-based Spearman and linear Pearson correlation coefficients are reported if data are normally distributed as assessed by Kolmogorov-Smirnov tests for normality). Furthermore, UPDRS-III scores pooled across stimulation conditions inversely correlated with movement velocity averaged across movement conditions (Fig. 2E; Spearman's rho = -0.55, $P < 0.001$; Pearson's R = -0.51, $P < 0.001$) and relative change in UPDRS-III scores [$\%UPDRS\text{-}III^{(off\text{-}on)/off}$] correlated with relative change in movement velocity (Fig. 2F). Pen-to-cursor mapping inversion in the controlled condition led to longer reaction times, indicating higher cognitive or inhibitory demand (Fig. 2D; $P < 0.0001$ for all participants). Patients with Parkinson's disease off stimulation reacted slower than healthy controls in both conditions ($P < 0.05$, unpaired permutation tests). Subthalamic stimulation led to a significant decrease in reaction times only in the controlled condition ($P < 0.001$) and to a significant decrease in reaction time adaptation defined as $\Delta RT^{controlled\text{-}automatic}$ compared to off stimulation ($P = 0.004$) and healthy controls ($P < 0.018$). When trial conditions were presented in random order (random block), reaction times were significantly reduced by DBS in both conditions, suggesting a general effect of DBS on reaction times under cognitive demand ($P < 0.05$, paired permutation test).

Reaction time modulation is correlated with the amount of cortico–subthalamic fibres affected by subthalamic stimulation

Average active contact location (Fig. 3A) was in remarkable proximity (0.8/1.2 mm on average for right/left hemisphere at a contact size of 1.5 mm length) to a previously published sweet spot for subthalamic DBS in Parkinson's disease derived from a meta-analysis of 466 electrode locations (Caire *et al.*, 2013; Horn *et al.*, 2017*a*), with all electrodes directly traversing the STN except for two trajectories in the left hemisphere that reside too far anterolateral (in Patients 1 and 13). DBS decreased the difference

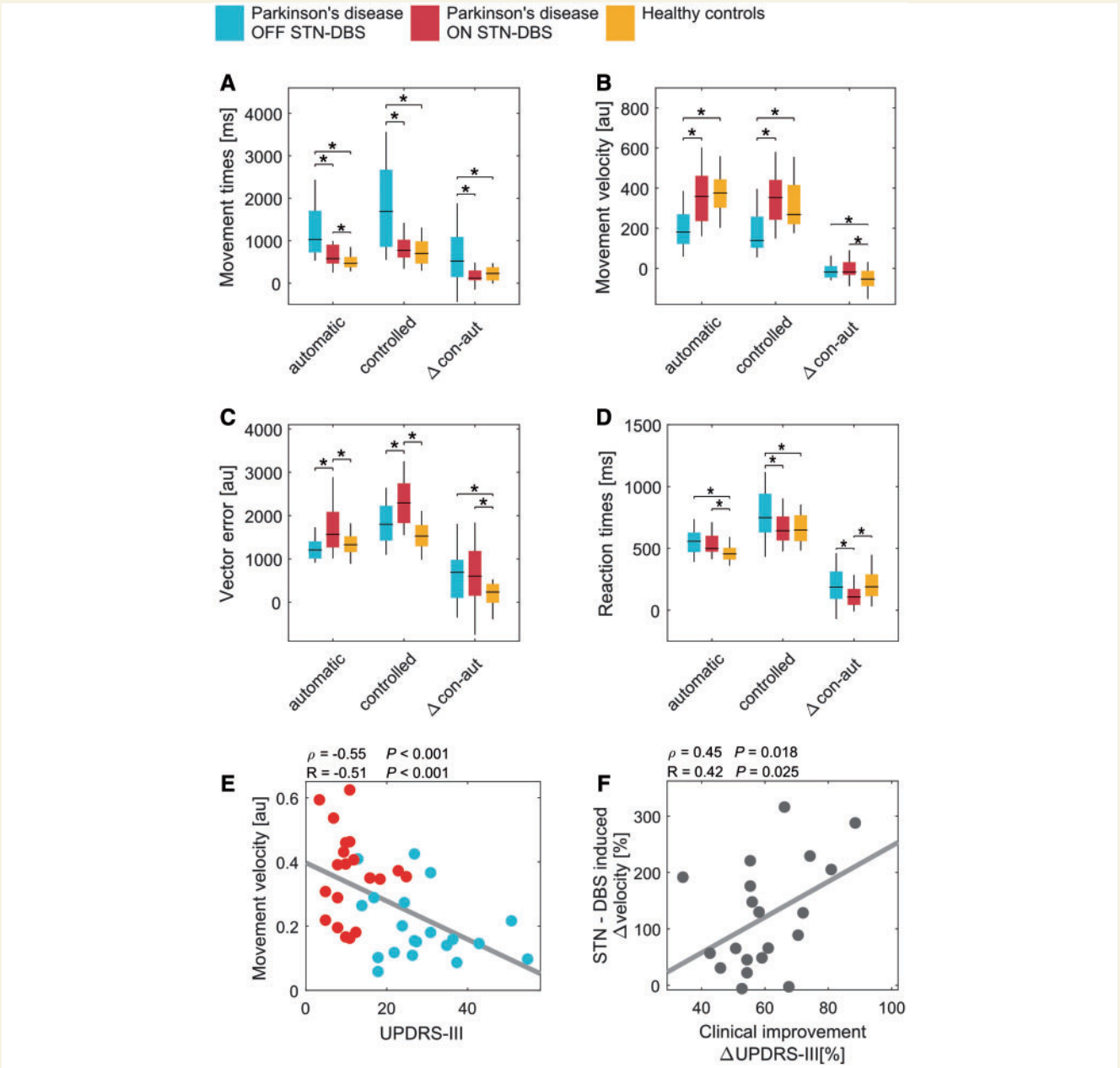

Figure 2 Behavioural results. Movement time (**A**), movement velocity (**B**), vector error (**C**) and reaction times (**D**) were extracted for each condition and for the difference between conditions from recorded movement trajectories and compared using permutation tests (box and whisker depict mean, error bars indicate SEM; *P-value < 0.05). Movement velocity values averaged across task conditions correlated significantly with UPDRS-III scores pooled across stimulation conditions (**E**) and relative change in each UPDRS-III and movement velocity (**F**).

between reaction times in the controlled and automatic condition by 41.29 ± 13.48% and this change correlated with the relative and absolute amount of hyperdirect pathway fibres (Fig. 3B and C) stimulated by the active DBS electrode across patients (Fig. 3D; Pearson's R = 0.56/0.59 P = 0.002/0.003; Spearman's rho = 0.54/0.49 P = 0.005/0.017, respectively). This effect was independent of the clinical motor DBS effect in UPDRS-III scores, levodopa equivalent dose (LEDD) and dopamine agonist therapy, which was controlled for using partial correlations. Moreover, direct comparison of the two subgroups of 10 age- and UPDRS-matched patients with Parkinson's disease (Group 1 DBS on/off; Group 2 levodopa ON/OFF) validated that DBS lead to a significantly greater reaction time change in the controlled condition, when compared to the effect of levodopa (P = 0.02; unpaired permutation test; Supplementary Fig. 1). Furthermore, no significant correlations were revealed for fibre counts with movement times ($P > 0.1$), UPDRS scores on stimulation ($P > 0.1$) or UPDRS improvement ($P > 0.1$). Thus, hyperdirect

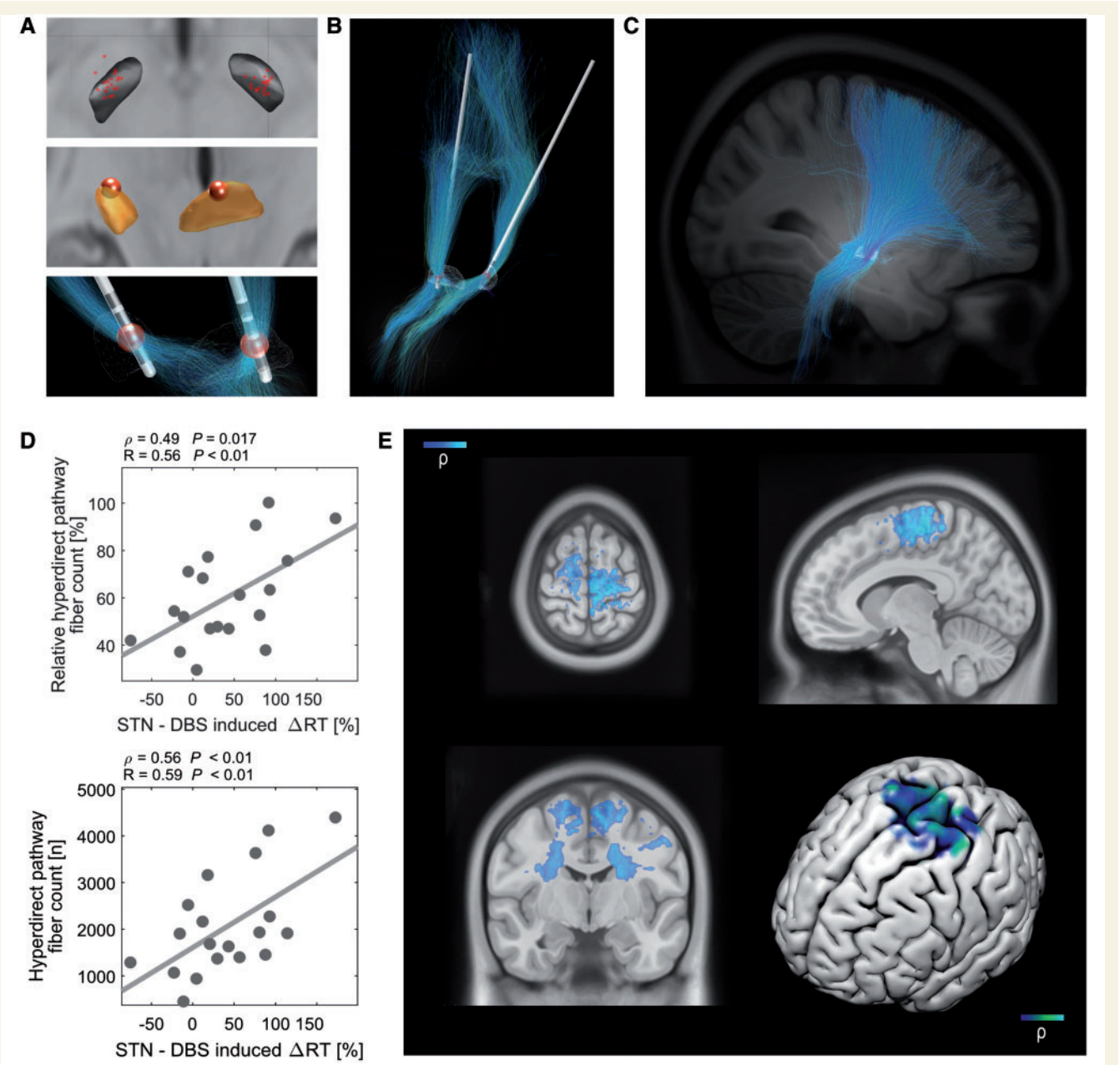

Figure 3 Fibre tracking from active deep brain stimulation contacts. All subthalamic deep brain stimulation electrodes were localized and transferred to MNI space (**A**) *Top*: All active contact locations; *middle*: average location of active contacts (0.8/1.2 mm distance to optimal target (Horn *et al.*, 2017*a*); and *bottom*: an example of the volume accounted for fibre tracking surrounding active contacts (red sphere). All fibres traversing the STN and the active contact were identified and selected from a whole-brain group connectome (**B**) resulting in a structural pathway (**C**; all fibres pooled across patients). A significant correlation of relative amount of sensorimotor cortex projecting fibres (depicted as hyperdirect pathway) to all fibres traversing the active contact (**D**) and absolute amount of sensorimotor cortex projecting fibres was found with the DBS induced % change in reaction time. Volumetric correlation analysis revealed a significant cluster in the medial frontal (**E**) cortex overlapping with the supplementary motor area (colour indicates correlation coefficient projected onto the T_1 template of the MNI brain, slice location is $x = -8$, $y = -6$, $z = 69.5$).

pathway fibre stimulation may specifically decrease reaction times under cognitive inhibitory demand leading to perturbed reaction time adaptation to task difficulty. Voxel-wise Spearman correlations of fibre density with the reaction time effect revealed a significant cluster in a mesial frontal location overlapping with the SMA that was visualized on the cortical surface (Fig. 3E; $P < 0.05$, cluster permutation corrected for multiple comparisons).

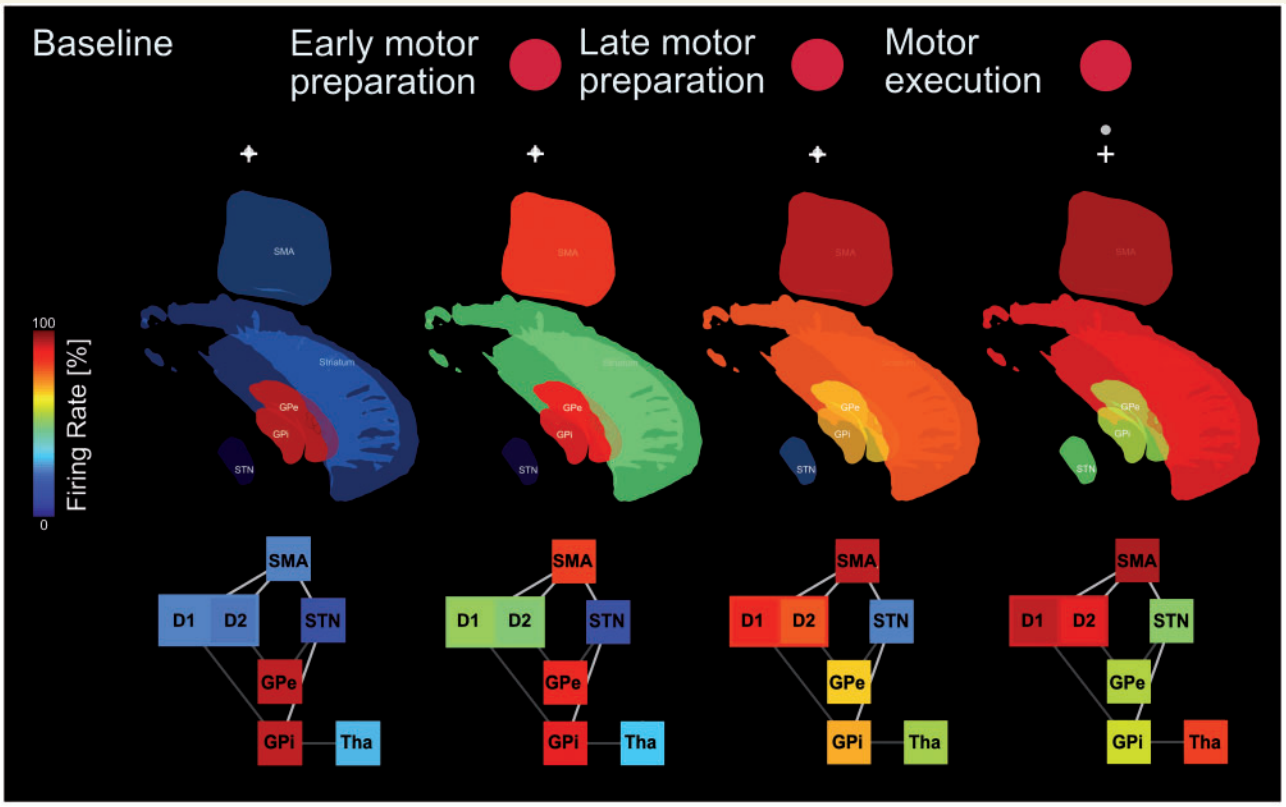

Figure 4 A firing rate model that can perform the task. A representative trial performed by the healthy basal ganglia model illustrates the core elements and network dynamics [task stage depicted on top as baseline (−500 ms in relation to cue onset), early motor preparation (250 ms), late motor preparation (500 ms) and during motor execution (1500 ms)]; 3D representations of model elements in the middle, 2D representations below, colour depicts relative baseline corrected firing rate (see Supplementary Video 1 for a recording of this model trial during task performance).

Computational basal ganglia modelling can predict the behavioural results of DBS induced dynamic circuit alterations in patients with Parkinson's disease

To test our hypotheses of differential indirect and hyperdirect pathway alterations through subthalamic DBS a computational model of the cortex–basal ganglia–thalamic circuit (adapted from Schroll *et al.*, 2014) was designed to simulate task-related basal ganglia activity *in silico* (Fig. 4). Model reaction times and movement times were determined by activity thresholds of the model's motor neurons depending on upstream computations of direct, indirect and hyperdirect basal ganglia pathways (Fig. 5A). To simulate the effects of Parkinson's disease, loss of dopamine was assumed to strengthen the indirect and weaken the direct pathway. Our model could correctly predict the reaction (Pearson's $R = 0.96$, $P < 0.0001$; Spearman's rho = 0.94, $P < 0.0001$) and movement times (Pearson's $R = 0.98$, $P < 0.0001$; Spearman's rho = 0.97, $P < 0.0001$) in patients with Parkinson's disease off stimulation and healthy controls (Pearson's $R = 0.82/0.46$, $P < 0.001/0.02$ and Spearman's rho = 0.89/0.51, $P < 0.0001/0.01$ for reaction/movement times, respectively). Next, pathway lesions were introduced to the computational basal ganglia loop to test the contributions of both the indirect and hyperdirect pathway to the DBS-related reaction time and movement time effects. The hyperdirect pathway lesion was modelled as a disruption of monosynaptic cortico-subthalamic signalling, whereas the indirect pathway lesion was introduced by disruption of cortical input to striatal D2 neurons with a consecutive increase in external globus pallidus activity and a subsequent increase in STN inhibition. Note, that this is a practical implementation of the finding that DBS induced motor sign alleviation are best explained by suppression of indirect pathway activity (Kahan *et al.*, 2014), which is further supported by the finding that parkinsonian symptom alleviation is correlated with local modulation of oscillatory activity, but not reduction in cortico-subthalamic connectivity (Oswal *et al.*, 2016). Stepwise regression model selection was conducted to find the lesion that best predicted the patients' behaviour on STN-DBS. In line with the fibre tracking results, the hyperdirect pathway lesion best predicted the patients on stimulation reaction time

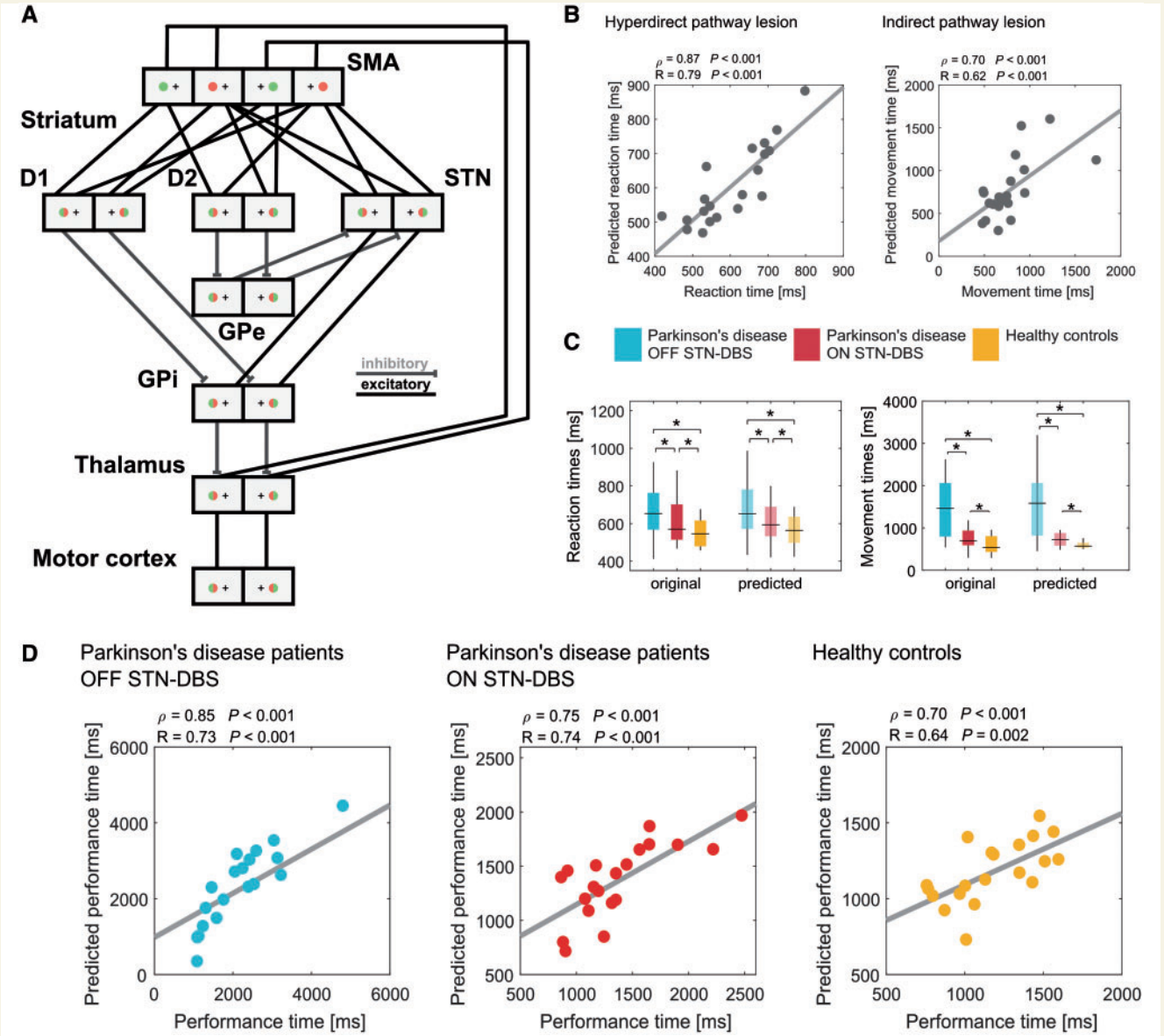

Figure 5 The computational basal ganglia model can predict task effects. The model architecture comprises a simplified version of the cortex–basal ganglia–thalamic loop (**A**). The model's SMA comprises four distinct neurons, each encoding a combination of stimulus type (red versus green circle) with spatial location (i.e. the location at which circles were shown with respect to the fixation cross in the unit; in our simulations we generalize across the exact circular angle providing only two options). The subsequent structures integrate the condition-specific activity in two cells (the striatum has two cells in each of the D1 and the D2 compartments), encoding the two spatial locations to which motor responses can be directed. The respective model computations result in different levels of motor cortex output that is directly translated into cursor movement. Lesions (**B**) of the hyperdirect pathway best predicted the reaction times during DBS (*left*; only results from leave one out cross-validation are shown throughout all panels), while lesions of the indirect pathway best predicted movement times (*right*). Overall, relevant original behavioural results (**C**) could be replicated by our models (shaded box and whisker; error bars depict SEM) for both reaction times (*left*) and movement times (*right*). All predictions were robust after leave-one-out cross validation, through which performance time (reaction time + movement time) of left out participants could be significantly predicted from the model of the remaining participants (**D**) for patients off (*left*) and on subthalamic DBS (*middle*) and healthy controls. D1 = striatal dopamine receptor 1 positive medium spiny neuron; D2 = striatal dopamine receptor 2 positive medium spiny neuron; GPi = internal pallidum.

results (estimated coefficient: 0.84, $R^2 = 0.71$, $P < 0.0001$, indirect pathway lesion data removed by stepwise model selection, hypothetical estimated coefficient: −1.1) in the stepwise model selection. For movement times, the indirect pathway lesion data best explained the patients on stimulation results (estimated coefficient: 0.7 $R^2 = 0.49$, $P < 0.001$, hyperdirect pathway lesion data removed by stepwise model selection, hypothetical estimated coefficient: −1.9).

Again, leave one out cross-validation was used to validate the predictive power of the linear regression model for the hyperdirect pathway lesion for reaction times (Fig. 5B; Pearson's $R = 0.79$, $P < 0.0001$; Spearman's rho = 0.87, $P < 0.0001$) and indirect pathway lesion for movement times (Pearson's $R = 0.62$, $P = 0.001$; Spearman's rho = 0.70 $P < 0.001$). Finally, to integrate all the reported findings of hyperdirect and indirect pathway modulations through subthalamic stimulation, we simulated subthalamic high frequency DBS in our model as a decrease of firing rate modulation of the STN leading to disruption of pallidal outflow from cortical hyperdirect and striatal indirect pathway activity, thus mimicking a depolarization block, which is a practical but likely simplistic account of the underlying therapeutic mechanism (Florence *et al.*, 2016). For our DBS simulation in the basal ganglia networks, the disruption of hyperdirect pathway signalling was dissociated from the disruption of indirect pathway input by weighting the hyperdirect pathway modulation by the amount of hyperdirect fibres stimulated in each case, whereas the indirect pathway modulation was weighted by the relative improvement in UPDRS-III scores. To investigate the predictive performance of our DBS model in comparison to hyperdirect and indirect pathway lesions, we included the DBS modelling results to the stepwise regression. Our combined hyperdirect and indirect pathway lesion (DBS) model outperformed the single pathway lesion models leading to improved estimations for both reaction (estimated coefficient: 0.84, $R^2 = 0.71$, $P < 0.0001$) and movement times (estimated coefficient: 0.76, $R^2 = 0.57$, $P = 0.0001$) and mildly improved leave one out cross-validation results (Pearson's $R = 0.79/0.69$ $P < 0.001/0.001$; Spearman's rho = 0.87/0.73 $P < 0.001/0.001$ for reaction/movement times, respectively) highlighting the interference of STN DBS with these pathways. Finally, we visualized the predictive power by running leave one out validation on the performance times (reaction + movement times) in patients off and on DBS and healthy controls. Reaction times, movement times and performance times are visualized separately in box and whisker plots and compared using permutation tests as mentioned above (Fig. 5C). After confirming the significance in normalized data, we reran the last analyses to estimate the true error in milliseconds to present meaningful values for the predicted times without prior transformation to a normal distribution (Fig. 5D). Average root mean squared errors were 40.6/45.7/40.8 ms (Parkinson's disease off/Parkinson's disease on/healthy controls, respectively) for reaction times, 309.0/240.7/153.2 ms (Parkinson's disease off/Parkinson's disease on/healthy controls, respectively) for movement times, and 569.18/221.27/172.9 ms (Parkinson's disease off/Parkinson's disease on/healthy controls, respectively) for performance times.

Discussion

We have shown that subthalamic DBS has differential effects on movement preparation and execution that could be explained by hyperdirect and indirect pathway functionality, respectively. First, behavioural results show that subthalamic DBS reduces the adaptation of reaction times to task demands, leading to faster but more erroneous movements. This was independent of the clinical motor sign improvement that was significantly correlated with modulation of movement velocity and movement time. Second, hyperdirect pathway fibre stimulation specifically decreased reaction times under cognitive inhibitory demand leading to faster reaction times, despite increased task difficulty. Finally, a computational model was able to explain both changes in reaction and movement times by means of hyperdirect and indirect pathway functionality. This suggests that DBS in Parkinson's disease modulates cognitive aspects of motor preparation through the hyperdirect pathway, in parallel with movement kinematics through the indirect pathway. Patients off DBS showed marked deterioration in task performance that was more pronounced in the condition that required cautious inhibitory motor control. DBS interfered with both cognitive and motor processing in the task and our findings integrate with previous reports regarding cognitive and clinical implications of distinct pathway effects in Parkinson's disease.

Before we move on with a detailed discussion of our findings on pathway-specific effects we should bear in mind that the present study was not intended or designed to identify the cellular mechanism of action of DBS. Hence, we will not claim that clinical efficacy does not depend at least in part of orthodromic or antidromic activation of white matter tracts, which is supported by several well conducted studies (Gradinaru *et al.*, 2009; Li *et al.*, 2012; Sanders and Jaeger, 2016). Fibre activation may be one of the underlying mechanisms of DBS that could result in local and distant network effects on subcortical and cortical levels, but the exact fibres implicated remain unknown. Importantly, this does not contradict a net suppression of subthalamic firing during DBS, which was recently demonstrated in patients with Parkinson's disease (Milosevic *et al.*, 2018) and could underlie the information block as modelled in the present study. Moreover, not only changes in firing rate but also temporal patterning of spike firing in the beta frequency range that has been shown to underlie the local representation of oscillatory beta activity (Kühn *et al.*, 2005) is considered an important factor in the pathophysiology of Parkinson's disease (Neumann *et al.*, 2016*a*, 2017; Geng *et al.*, 2017; Steiner *et al.*, 2017; Tinkhauser *et al.*, 2017). Our model does not incorporate beta oscillations as this would add significantly to the model complexity with many assumptions that remain to be established. However, we would like to point out that subthalamic beta oscillations have shown to parallel an increase in firing rates associated with the hypodopaminergic state in the MPTP-treated monkey, while pharmacological lesioning of the STN was shown to reduce both, STN firing rates and beta activity (Tachibana *et al.*, 2011). Indeed, suppression of beta activity through DBS (Kühn *et al.*, 2008; Neumann *et al.*, 2016*b*) was recently proposed to rely on

synaptic silencing, leading to reduced subthalamic firing rates (Milosevic *et al.*, 2018). Thus, the implemented rate changes can be interpreted as the foundation for more complex basal ganglia models including temporal patterning in the beta range (Pavlides *et al.*, 2015) that should be integrated in future studies but can be interpreted as complimentary mechanisms that do not contradict each other.

The following discussion will aim to explain the functional consequences of subthalamic DBS in relation to previous findings on the cortex–basal ganglia–thalamic loop.

The role of the hyperdirect pathway has best been studied in the cognitive domain where the STN is proposed to elevate decision thresholds under conflict to optimize behavioural outcome (Frank *et al.*, 2007; Green *et al.*, 2013) potentially through communication in low frequency oscillations (Cavanagh *et al.*, 2011; Herz *et al.*, 2016). Subthalamic DBS interferes with this function leading to impulsive and consequently suboptimal choices or increased error rates. Our study extends these findings to the (pre)-motor domain, as patients in our task were preparing for a complex movement rather than indicating binary choices with a single button press. While reaction times were significantly slower when DBS was turned off, the adaptation of reaction times to the more difficult task condition was not significantly different to that of healthy controls—indicating a normal but shifted reaction time adaptation in Parkinson's disease. DBS specifically reduced the reaction time adaptation, i.e. reduced the reaction time relatively more in the controlled as opposed to automated motor task. This DBS effect increased with proximity of the active contact to cortico-subthalamic fibres connecting the medial frontal cortex or SMA with the STN that are part of a postulated inhibition triangle (Aron *et al.*, 2007). The STN and SMA have previously been implicated in switching from automatic to controlled behaviour in a similar experiment on saccades and antisaccades in trained macaques (Isoda and Hikosaka, 2007, 2008, 2011). Neurons in the medial frontal cortex were reported to be active during switching from automatic saccades to controlled antisaccades and stimulation of SMA replaced automatic incorrect responses with slower correct responses (Isoda and Hikosaka, 2007). In the STN, specific neurons were identified that are activated during the preparation of controlled antisaccades, potentially reflecting a suppression of the automatic response (Isoda and Hikosaka, 2008). This observation in combination with the fact that suppression of hyperdirect pathway activity to the STN in the model best predicted reaction times of our patients on DBS supports the hypothesis that decreased reaction time adaptation through stimulation may be mediated by interfering with hyperdirect pathway communication to the STN.

Neither the reported reaction time effects, nor the amount of SMA–subthalamic fibres in relation to all fibres in proximity to active DBS contacts showed a significant association with clinical motor sign alleviation, which was in contrast correlated with movement time and velocity. This point is crucial, since it differentiates the hyperdirect mediated effect from general symptom improvements and demonstrates that the pathway is likely responsible for a specific behavioural phenomenon that does not share significant variance with pure motor improvement as measured by UPDRS. Increased movement velocity and decreased movement times in the DBS on condition may thus reflect a modulation of subcortical neurotransmission to the STN that to a certain degree is independent from monosynaptic cortical input. Indeed, cortico–subthalamic hyperdirect pathway input has recently been reported to decrease in the parkinsonian state due to increased striatopallidal transmission (Chu *et al.*, 2017). The computational model demonstrated best predictions on movement times on DBS through a suppression of the indirect pathway in our patients. In this regard, optogenetic manipulation of basal ganglia circuitry reported optogenetic excitation of indirect pathway MSNs to be sufficient to elicit parkinsonian symptoms in healthy rodents, whereas direct pathway activation could alleviate motor symptoms in a mouse model of Parkinson's disease (Kravitz *et al.*, 2010). In fact, cell-specific excitation of Parvalbumin positive neurons in the external pallidum alone was shown to produce marked movement restoration in parallel with attenuation of pathological activity in basal ganglia output nuclei in dopamine depleted mice (Mastro *et al.*, 2017).

Furthermore, investigation of pathway-specific DBS effects in patients with Parkinson's disease through dynamic causal modelling in resting state functional MRI has proposed that the clinical state was best explained by increased indirect pathway activity and that DBS-related symptom alleviation correlated with a reduction of the latter (Kahan *et al.*, 2014). Furthermore, observations on cortico–subcortical oscillatory circuit dynamics through parallel subthalamic local field potential and whole head magnetoencephalography suggest that suppression of subthalamic low beta activity correlates with DBS related motor improvement, but not modulation of cortico–subthalamic high beta connectivity, which was proposed to reflect hyperdirect pathway coupling in analyses of conduction delays (Oswal *et al.*, 2016). In the present study, patients with Parkinson's disease were more impaired in the controlled condition of our task requiring increased motor control. This effect may be related to the role of the basal ganglia in motor skill acquisition and procedural learning (Jog *et al.*, 1999), where well-trained actions may become less dopamine dependent and therefore less affected in the parkinsonian state (Choi *et al.*, 2005). In contrast, dopamine seems critical for the formation of habit and automaticity (Graybiel, 2008). Importantly, DBS did not improve movement velocity adaptation via slowing of movement to cope with increased task difficulty in the controlled condition, which in fact may reflect the loss of an important physiological function of the basal ganglia not restored through continuous DBS. Remarkably, optogenetic manipulations of indirect pathway neurons were sufficient to decrease and increase movement velocity during task performance in healthy mice (Yttri and Dudman, 2016). In

this regard, subthalamic oscillatory activity was recently demonstrated to encode movement velocity in dependence of dopamine in human patients with Parkinson's disease, providing a link between kinematic motor control and symptoms of bradykinesia in the hypodopaminergic state (Lofredi *et al.*, 2018).

It is likely that DBS effects are transmitted not by a single mechanism of action but multiple interactions from molecular and cellular processes translating into global network effects that also span different time scales. Here, potentially complementary mechanisms to the depolarization block, implemented in our computational model, have been proposed, such as regularization of aberrant activity, modulation of extracellular ions and neurotransmitters and axonal activation (Florence *et al.*, 2016; Wichmann and DeLong, 2016). Each proposed mechanism would likely yield complex interactions with both hyperdirect and indirect pathways. Cognitive and motor effects of DBS may result from modulation of converging neural pathways in the STN and are impossible to disentangle with certainty. Similarly, the classic rate model does not account for all observed behavioural effects through optogenetic stimulation, as the indirect pathway and direct pathway have both been shown to be involved in action initiation and execution (Cui *et al.*, 2013; Tecuapetla *et al.*, 2016). Notwithstanding this, our study aims at providing a framework to explain pathway-linked DBS effects that may guide innovation to improve therapeutic success in patients with Parkinson's disease. Adaptive closed loop DBS approaches are now in development in the hope to improve therapeutic efficacy and reduce adverse effects and first studies have shown promising results (Little *et al.*, 2013) using subthalamic beta synchronization that can reflect parkinsonian symptom severity in the STN (Kühn *et al.*, 2006; Neumann *et al.*, 2016*a*, 2017) or potentially cortical phase amplitude coupling (de Hemptinne *et al.*, 2013, 2015; Swann *et al.*, 2015, 2018) to trigger stimulation. Based on our findings, we propose that innovative therapeutic neuromodulation approaches should aim to adapt stimulation not only to symptom severity, but also to physiological signals reflecting inhibitory cognitive and motor demand to re-enable flexible motor control. We propose that computational basal ganglia models could serve as neural prosthetics to control subthalamic inhibitory output based on complex input signals derived from cortical, subcortical and peripheral sensors. Crucially, the model devised in the present manuscript only requires clinically abundant parameters (UPDRS-III in off state, pre- and postoperative imaging) to make predictions about behavioural DBS effects that go above and beyond pure motor sign improvements and may be able to further fine-tune optimal stimulation parameters in DBS programming in the future.

Acknowledgements

Data used in the preparation of this article were obtained from the Parkinson's Progression Markers Initiative (PPMI) database (www.ppmi-info.org/data). For up-to-date information on the study, visit www.ppmi-info.org. PPMI–a public-private partnership–is funded by the Michael J. Fox Foundation for Parkinson's Research and funding partners, see www.ppmi-info.org/fundingpartners.

Funding

The study has been funded by the German Research Foundation (DFG grant KFO 247).

Competing interests

The authors report no competing interests.

Supplementary material

Supplementary material is available at *Brain* online.

References

Albin RL, Young AB, Penney JB. The functional anatomy of basal ganglia disorders. Trends Neurosci 1989; 12: 366–75.

Aron AR, Behrens TE, Smith S, Frank MJ, Poldrack RA. Triangulating a cognitive control network using diffusion-weighted magnetic resonance imaging (MRI) and functional MRI. J Neurosci 2007; 27: 3743–52.

Aron AR, Herz DM, Brown P, Forstmann BU, Zaghloul K. Frontosubthalamic circuits for control of action and cognition. J Neurosci 2016; 36: 11489–95.

Ashburner J, Friston KJ. Unified segmentation. Neuroimage 2005; 26: 839–51.

Ashburner J, Friston KJ. Diffeomorphic registration using geodesic shooting and Gauss-Newton optimisation. Neuroimage 2011; 55: 954–67.

Benjamini Y, Krieger AM, Yekutieli D. Adaptive linear step-up procedures that control the false discovery rate. Biometrika 2006; 93: 491–507.

Bergman H, Wichmann T, DeLong MR. Reversal of experimental parkinsonism by lesions of the subthalamic nucleus. Science 1990; 249: 1436–8.

Caire F, Ranoux D, Guehl D, Burbaud P, Cuny E. A systematic review of studies on anatomical position of electrode contacts used for chronic subthalamic stimulation in Parkinson's disease. Acta Neurochir 2013; 155: 1647–54.

Cavanagh JF, Wiecki TV, Cohen MX, Figueroa CM, Samanta J, Sherman SJ, et al. Subthalamic nucleus stimulation reverses mediofrontal influence over decision threshold. Nat Neurosci 2011; 14: 1462–7.

Choi WY, Balsam PD, Horvitz JC. Extended habit training reduces dopamine mediation of appetitive response expression. J Neurosci 2005; 25: 6729–33.

Chu HY, McIver EL, Kovaleski RF, Atherton JF, Bevan MD. Loss of Hyperdirect pathway cortico-subthalamic inputs following degeneration of midbrain dopamine neurons. Neuron 2017; 95: 1306–18.e5.

Cui G, Jun SB, Jin X, Pham MD, Vogel SS, Lovinger DM, et al. Concurrent activation of striatal direct and indirect pathways during action initiation. Nature 2013; 494: 238–42.

de Hemptinne C, Ryapolova-Webb ES, Air EL, Garcia PA, Miller KJ, Ojemann JG, et al. Exaggerated phase-amplitude coupling in the primary motor cortex in Parkinson disease. Proc Natl Acad Sci USA 2013; 110: 4780–5.

de Hemptinne C, Swann NC, Ostrem JL, Ryapolova-Webb ES, San Luciano M, Galifianakis NB, et al. Therapeutic deep brain stimulation reduces cortical phase-amplitude coupling in Parkinson's disease. Nat Neurosci 2015; 18: 779–86.

DeLong MR. Primate models of movement disorders of basal ganglia origin. Trends Neurosci 1990; 13: 281–5.

Deuschl G, Schade-Brittinger C, Krack P, Volkmann J, Schafer H, Botzel K, et al. A randomized trial of deep-brain stimulation for Parkinson's disease. N Engl J Med 2006; 355: 896–908.

Ewert S, Plettig P, Li N, Chakravarty MM, Collins DL, Herrington TM, et al. Toward defining deep brain stimulation targets in MNI space: a subcortical atlas based on multimodal MRI, histology and structural connectivity. Neuroimage 2018; 170: 271–82.

Florence G, Sameshima K, Fonoff ET, Hamani C. Deep brain stimulation: more complex than the inhibition of cells and excitation of fibers. Neuroscientist 2016; 22: 332–45.

Fox MD, Buckner RL, Liu H, Chakravarty MM, Lozano AM, Pascual-Leone A. Resting-state networks link invasive and noninvasive brain stimulation across diverse psychiatric and neurological diseases. Proc Natl Acad Sci USA 2014; 111: E4367–75.

Frank MJ, Samanta J, Moustafa AA, Sherman SJ. Hold your horses: impulsivity, deep brain stimulation, and medication in parkinsonism. Science 2007; 318: 1309–12.

Geng X, Zhang J, Jiang Y, Ashkan K, Foltynie T, Limousin P, et al. Comparison of oscillatory activity in subthalamic nucleus in Parkinson's disease and dystonia. Neurobiol Dis 2017; 98: 100–7.

Gradinaru V, Mogri M, Thompson KR, Henderson JM, Deisseroth K. Optical deconstruction of parkinsonian neural circuitry. Science 2009; 324: 354–9.

Graybiel AM. Habits, rituals, and the evaluative brain. Annu Rev Neurosci 2008; 31: 359–87.

Green N, Bogacz R, Huebl J, Beyer AK, Kühn AA, Heekeren HR. Reduction of influence of task difficulty on perceptual decision making by STN deep brain stimulation. Curr Biol 2013; 23: 1681–4.

Herz DM, Little S, Pedrosa DJ, Tinkhauser G, Cheeran B, Foltynie T, et al. Mechanisms underlying decision-making as revealed by deep-brain stimulation in patients with Parkinson's disease. Curr Biol 2018; 28: 1169–78.e6.

Herz DM, Zavala BA, Bogacz R, Brown P. Neural correlates of decision thresholds in the human subthalamic nucleus. Curr Biol 2016; 26: 916–20.

Horn A, Kühn AA. Lead-DBS: a toolbox for deep brain stimulation electrode localizations and visualizations. Neuroimage 2015; 107: 127–35.

Horn A, Kühn AA, Merkl A, Shih L, Alterman R, Fox M. Probabilistic conversion of neurosurgical DBS electrode coordinates into MNI space. Neuroimage 2017a; 150: 395–404.

Horn A, Neumann WJ, Degen K, Schneider GH, Kühn AA. Toward an electrophysiological "sweet spot" for deep brain stimulation in the subthalamic nucleus. Hum Brain Mapp 2017b; 38: 3377–90.

Horn A, Ostwald D, Reisert M, Blankenburg F. The structural-functional connectome and the default mode network of the human brain. Neuroimage 2014; 102 (Pt 1): 142–51.

Horn A, Reich M, Vorwerk J, Li N, Wenzel G, Fang Q, et al. Connectivity Predicts deep brain stimulation outcome in Parkinson disease. Ann Neurol 2017c; 82: 67–78.

Isoda M, Hikosaka O. Switching from automatic to controlled action by monkey medial frontal cortex. Nat Neurosci 2007; 10: 240–8.

Isoda M, Hikosaka O. Role for subthalamic nucleus neurons in switching from automatic to controlled eye movement. J Neurosci 2008; 28: 7209–18.

Isoda M, Hikosaka O. Cortico-basal ganglia mechanisms for overcoming innate, habitual and motivational behaviors. Eur J Neurosci 2011; 33: 2058–69.

Jahanshahi M, Obeso I, Rothwell JC, Obeso JA. A fronto-striato-subthalamic-pallidal network for goal-directed and habitual inhibition. Nat Rev Neurosci 2015; 16: 719–32.

Jog MS, Kubota Y, Connolly CI, Hillegaart V, Graybiel AM. Building neural representations of habits. Science 1999; 286: 1745–9.

Kahan J, Urner M, Moran R, Flandin G, Marreiros A, Mancini L, et al. Resting state functional MRI in Parkinson's disease: the impact of deep brain stimulation on 'effective' connectivity. Brain 2014; 137: 1130–44.

Kravitz AV, Freeze BS, Parker PR, Kay K, Thwin MT, Deisseroth K, et al. Regulation of parkinsonian motor behaviours by optogenetic control of basal ganglia circuitry. Nature 2010; 466: 622–6.

Kühn AA, Kupsch A, Schneider GH, Brown P. Reduction in subthalamic 8–35 Hz oscillatory activity correlates with clinical improvement in Parkinson's disease. Eur J Neurosci 2006; 23: 1956–60.

Kühn AA, Trottenberg T, Kivi A, Kupsch A, Schneider GH, Brown P. The relationship between local field potential and neuronal discharge in the subthalamic nucleus of patients with Parkinson's disease. Exp Neurol 2005; 194: 212–20.

Kühn AA, Kempf F, Brücke C, Gaynor Doyle L, Martinez-Torres I, Pogosyan A, et al. High-frequency stimulation of the subthalamic nucleus suppresses oscillatory beta activity in patients with Parkinson's disease in parallel with improvement in motor performance. J Neurosci 2008; 28: 6165–73.

Lee JH, Kreitzer AC, Singer AC, Schiff ND. Illuminating neural circuits: from molecules to MRI. J Neurosci 2017; 37: 10817–25.

Li Q, Ke Y, Chan DC, Qian ZM, Yung KK, Ko H, et al. Therapeutic deep brain stimulation in Parkinsonian rats directly influences motor cortex. Neuron 2012; 76: 1030–41.

Little S, Pogosyan A, Neal S, Zavala B, Zrinzo L, Hariz M, et al. Adaptive deep brain stimulation in advanced Parkinson disease. Ann Neurol 2013; 74: 449–57.

Lofredi R, Neumann WJ, Bock A, Horn A, Huebl J, Siegert S, et al. Dopamine-dependent scaling of subthalamic gamma bursts with movement velocity in patients with Parkinson's disease. Elife 2018; 7: e31895.

Marek K, Jennings D, Lasch S, Siderowf A, Tanner C, Simuni T, et al. The Parkinson Progression Marker Initiative (PPMI). Prog Neurobiol 2011; 95: 629–35.

Mastro KJ, Zitelli KT, Willard AM, Leblanc KH, Kravitz AV, Gittis AH. Cell-specific pallidal intervention induces long-lasting motor recovery in dopamine-depleted mice. Nat Neurosci 2017; 20: 815–23.

Milosevic L, Kalia SK, Hodaie M, Lozano AM, Fasano A, Popovic MR, et al. Neuronal inhibition and synaptic plasticity of basal ganglia neurons in Parkinson's disease. Brain 2018; 141: 177–90.

Nambu A, Tokuno H, Takada M. Functional significance of the cortico-subthalamo-pallidal 'hyperdirect' pathway. Neurosci Res 2002; 43: 111–17.

Neumann WJ, Degen K, Schneider GH, Brucke C, Huebl J, Brown P, et al. Subthalamic synchronized oscillatory activity correlates with motor impairment in patients with Parkinson's disease. Mov Disord 2016a; 31: 1748–51.

Neumann WJ, Staub F, Horn A, Schanda J, Mueller J, Schneider GH, et al. Deep brain recordings using an implanted pulse generator in Parkinson's disease. Neuromodulation 2016b; 19: 20–4.

Neumann WJ, Staub-Bartelt F, Horn A, Schanda J, Schneider GH, Brown P, et al. Long term correlation of subthalamic beta band activity with motor impairment in patients with Parkinson's disease. Clin Neurophysiol 2017; 128: 2286–91.

Oswal A, Beudel M, Zrinzo L, Limousin P, Hariz M, Foltynie T, et al. Deep brain stimulation modulates synchrony within spatially and spectrally distinct resting state networks in Parkinson's disease. Brain 2016; 139: 1482–96.

Pavlides A, Hogan SJ, Bogacz R. Computational models describing possible mechanisms for generation of excessive beta oscillations in Parkinson's disease. PLoS Comput Biol 2015; 11: e1004609.

Sanders TH, Jaeger D. Optogenetic stimulation of cortico-subthalamic projections is sufficient to ameliorate bradykinesia in 6-ohda lesioned mice. Neurobiol Dis 2016; 95: 225–37.

Schroll H, Hamker FH. Basal Ganglia dysfunctions in movement disorders: what can be learned from computational simulations. Mov Disord 2016; 31: 1591–601.

Schroll H, Vitay J, Hamker FH. Dysfunctional and compensatory synaptic plasticity in Parkinson's disease. Eur J Neurosci 2014; 39: 688–702.

Schuepbach WM, Rau J, Knudsen K, Volkmann J, Krack P, Timmermann L, et al. Neurostimulation for Parkinson's disease with early motor complications. N Engl J Med 2013; 368: 610–22.

Steiner LA, Neumann WJ, Staub-Bartelt F, Herz DM, Tan H, Pogosyan A, et al. Subthalamic beta dynamics mirror Parkinsonian bradykinesia months after neurostimulator implantation. Mov Disord 2017; 32: 1183–90.

Swann NC, de Hemptinne C, Aron AR, Ostrem JL, Knight RT, Starr PA. Elevated synchrony in Parkinson disease detected with electroencephalography. Ann Neurol 2015; 78: 742–50.

Swann NC, de Hemptinne C, Miocinovic S, Qasim S, Ostrem JL, Galifianakis NB, et al. Chronic multisite brain recordings from a totally implantable bidirectional neural interface: experience in 5 patients with Parkinson's disease. J Neurosurg 2018; 128: 605–16.

Tachibana Y, Iwamuro H, Kita H, Takada M, Nambu A. Subthalamopallidal interactions underlying parkinsonian neuronal oscillations in the primate basal ganglia. Eur J Neurosci 2011; 34: 1470–84.

Tecuapetla F, Jin X, Lima SQ, Costa RM. Complementary contributions of striatal projection pathways to action initiation and execution. Cell 2016; 166: 703–15.

Tinkhauser G, Pogosyan A, Little S, Beudel M, Herz DM, Tan H, et al. The modulatory effect of adaptive deep brain stimulation on beta bursts in Parkinson's disease. Brain 2017; 140: 1053–67.

Tzourio-Mazoyer N, Landeau B, Papathanassiou D, Crivello F, Etard O, Delcroix N, et al. Automated anatomical labeling of activations in SPM using a macroscopic anatomical parcellation of the MNI MRI single-subject brain. Neuroimage 2002; 15: 273–89.

van Albada SJ, Robinson PA. Transformation of arbitrary distributions to the normal distribution with application to EEG test-retest reliability. J Neurosci Methods 2007; 161: 205–11.

Weaver FM, Follett K, Stern M, Hur K, Harris C, Marks WJ, Jr., et al. Bilateral deep brain stimulation vs best medical therapy for patients with advanced Parkinson disease: a randomized controlled trial. JAMA 2009; 301: 63–73.

Wichmann T, DeLong MR. Functional and pathophysiological models of the basal ganglia. Curr Opin Neurobiol 1996; 6: 751–8.

Wichmann T, DeLong MR. Deep brain stimulation for movement disorders of Basal ganglia origin: restoring function or functionality? Neurotherapeutics 2016; 13: 264–83.

Yttri EA, Dudman JT. Opponent and bidirectional control of movement velocity in the basal ganglia. Nature 2016; 533: 402–6.